Structural, thermal, transport, and magnetic properties of the charge-ordered $La_{1/3}Ca_{2/3}MnO_3$ oxide

M. T. Fernández-Díaz
Institut Max Von Laue-Paul Langevin, BP 156, F-38042 Grenoble Cedex 9, France

J. L. Martínez and J. M. Alonso
Instituto de Ciencia de Materiales de Madrid, CSIC, Cantoblanco, E-28049 Madrid, Spain

E. Herrero
Departamento Química Inorgánica, Facultad C. Químicas Universidad Complutense, E-28040 Madrid, Spain

(Received 1 April 1998)

The compound $La_{1/3}Ca_{2/3}MnO_3$ has been studied in the temperature range from 1.5 to 400 K. The anomalous behavior of the resistivity, magnetic susceptibility, specific heat, and lattice parameters are the signature of a charge-ordering transition taking place at around 270 K. A structural model of this charge-ordered state is developed with a crystallographic unit cell given by $(3a\times b\times c)$ of the high-temperature unit cell and the same *Pbnm* symmetry. At 170 K an antiferromagnetic transition is clearly established on the magnetic susceptibility, resistivity, and specific heat. Neutron diffraction shows that the Mn magnetic moments order antiferromagnetically with a propagation vector $\mathbf{k}=(0,1/2,0)$. The observed magnetic configuration belongs to one of the two bidimensional representations of the group *Pbnm* associated with $\mathbf{k}=(0,1/2,0)$. [S0163-1829(99)02902-1]

INTRODUCTION

Hole-doped manganese oxides of perovskite type $R_{1-x}A_xMnO_3$ where R and A are trivalent rare earth and divalent alkaline earth, respectively, are highly correlated electron systems in which a close interplay of structural, transport, and magnetic properties gives rise to a complex phase diagram. Even if the main features of these phase diagrams have been established in the 1950s,[1,2] their interesting complexity makes a more profound characterization worthwhile.

The $x=0$ compound is antiferromagnetic and it shows orbital ordering due to a cooperative Jahn-Teller effect. Substitution of La by a divalent cation oxidizes Mn^{+3} to Mn^{+4}, introducing holes in the d band allowing the hopping of the e_g electron of a Mn^{+3} ion to the corresponding hole of a neighboring Mn^{+4}. This double exchange mechanism favors ferromagnetic interactions and leads to great enhancement of the conductivity below the Curie temperature.[3–7]

Besides the known negative magnetoresistance effect,[8] this family of compounds presents another interesting phenomenon which is the real-space ordering of charge carriers when the long-range Coulomb interaction between carriers overcomes their kinetic energy. It was suggested by Wollan and Koeller[2] that ordering of alternate Mn^{+3} and Mn^{+4} in a Nacl-like lattice would take place for compositions near $x=0.5$. A few years ago, Tomioka *et al.*[9] observed a transition from a ferromagnetic metal to an antiferromagnetic insulator on cooling. This transition can be suppressed by the application of a magnetic field. The spin-lattice coupling responsible for this latter phenomenon was also found by the same research group to be present in the $La_{1-x}Sr_xMnO_3$ system in which the orthorhombic-rhombohedral structural transition was monitored by application of a magnetic field.[10]

Yamada *et al.*[11] reported the existence of a polaron ordered phase at low-doping rates in $La_{1-x}Sr_xMnO_3$ with $x=1/8$, where holes freeze on the lattice sites. The onset of the polaron order coincides with the point of upturn in the resistivity. Such ordering of polarons has also been reported for hole-doped transition-metal oxides with layered perovskite structures, such as $La_{2-x}Sr_xNiO_4$ ($x=1/3$ and $1/2$),[12] $La_{2-x}Sr_xCuO_4$ ($x=1/8$),[13] and $La_{1-x}Sr_{1+x}MnO_4$ ($x=1/2$).[14]

More recently, real-space charge ordering has been inferred from electron-diffraction experiments on $La_{1-x}Ca_xMnO_3$ in the concentration range $0.63<x<0.67$ by Ramirez *et al.*[15] Similar results have been published by Chen *et al.*[16] and Mori *et al.*[17] on the $x=2/3$ compound using electron diffraction. None of these publications give a quantitative analysis of the charge-ordering state, but they propose models from the geometric characteristic of the electron diffraction pattern.

From these examples, it seems that the charge-ordered state is observed when the carrier concentration is a certain fraction of the number of lattice points, as if the commensurability of the hole concentration may be essential for the existence of a low-temperature charge-ordering transition.

In this paper we present a study of the structural, magnetic, and transport behavior of $La_{1/3}Ca_{2/3}MnO_3$ from 400 to 1.5 K. We present quantitative support for a particular charge-ordering state that can be deduced from the analysis of the magnetic state of the sample.

EXPERIMENT

The synthesis was performed by the classical ceramic method by annealing the stoichiometric amounts of the corresponding oxides for 72 h at 1400 °C in air. The resulting material was characterized by ICP (induce coupling plasma), thermogravimetric analysis, and x-ray diffraction confirming the nominal composition. The chemical analysis also shows

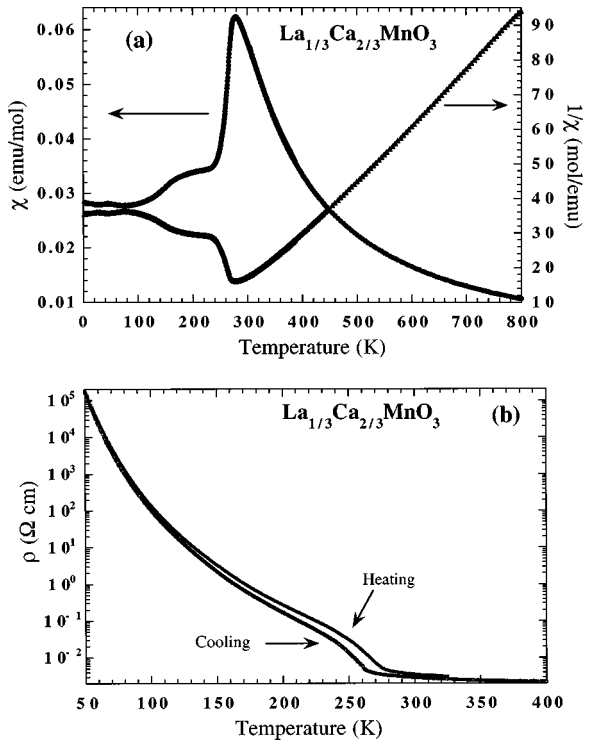

FIG. 1. (a) Temperature dependence of the magnetic susceptibility. (b) Thermal dependence of the electrical resistivity.

that the anionic lattice is complete.

Susceptibility measurements were performed in a SQUID magnetometer (QD-MPMS-5S) in the temperature range from 1.8 to 800 K, under an applied magnetic field of 0.1 T. The resistance measurements were performed by the four probe method in a temperature range from 5 to 400 K with an applied constant current of 1 mA. The specific heat was measured by the adiabatic heat pulse method in a temperature range from 2 to 400 K, and an applied external magnetic field up to 9 T (QD-PPMS system).

Neutron powder diffraction was performed at the ILL. Diffraction data were collected on the high resolution powder diffractometer D2B at 300, 200, and 1.5 K, using a wavelength of 1.594 Å. A temperature scan was made while warming from 1.5 to 300 K on the high flux powder diffractometer D1B, with a wavelength of 2.52 Å, in order to follow the evolution of the magnetic structure and the dependence of the lattice parameters on temperature. The Rietveld method was applied to refine the crystal and magnetic structure using the program FULLPROF.[18]

RESULTS

The temperature dependence of the magnetic susceptibility and the electrical resistivity are shown in Fig. 1, parts (a) and (b), respectively. It can be noticed that on cooling from high temperature, there is an increase of the magnetic susceptibility. The inverse susceptibility plot leads to a positive Weiss constant θ_W, indicating ferromagnetic interactions at high temperature.

The observed continuous increase in the magnetic susceptibility may correspond to a double-exchange interaction between Mn^{+3} and Mn^{+4} ions. As no magnetic contribution in the neutron diffraction data at RT is observed, it is supposed

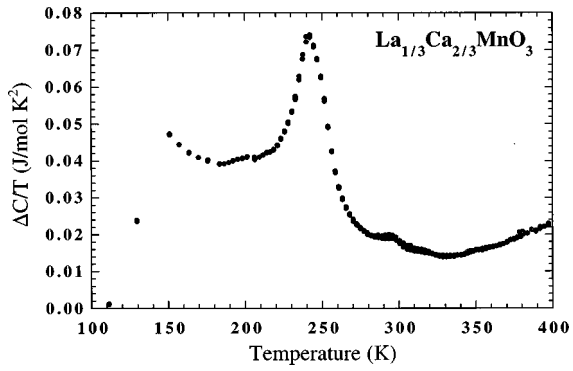

FIG. 2. Electronic and magnetic specific heat vs temperature in $La_{1/3}Ca_{2/3}MnO_3$.

that the corresponding ferromagnetic interactions have a very short correlation length; this is in agreement with the measured value of $\rho > 10^{-2}$ Ω cm which indicates an electron mean free path of a few Å. This could also be the reason for the lack of the linear Curie-Weiss behavior of the inverse magnetic susceptibility until high temperatures. The paramagnetic moment calculated for a temperature range from 450 to 800 K is $7.0\mu_B$, which is roughly double than expected for the mixture of $2/3\,Mn^{+4}$ and $1/3\,Mn^{+3}$. This failure of the Curie-Weiss model could be related to the short range ferromagnetic fluctuations and/or the inadequacy of the local moments approximation.

At 270 K the magnetic susceptibility reaches its maximum value, and below that temperature χ drops rapidly while ρ rises from the same temperature value. At lower temperature there is a broad maximum in the magnetic susceptibility, related to the long range antiferromagnetic order ($T_N \approx 170$ K).

Resistivity measurements have also been carried out under an external applied magnetic field on heating. Unlike the spectacular change in the resistivity observed in $Pr_{1/2}Sr_{1/2}MnO_3$ with the applied magnetic field,[9] in this compound the charge-ordered state is stable under an external applied magnetic field of 9 T. However, a hysteresis effect can be observed in the resistivity data on cooling and warming, indicating a first order character of the charge-ordering transition. The activation energy from the resistivity data at the high-temperature range ($T > 300$ K) is 27 meV.

To shed some light on the origin of these special features of the macroscopic magnetic susceptibility and transport measurements, specific heat and neutron powder-diffraction measurements have been carried out.

In order to analyze the relevant electronic and magnetic contributions to the specific heat data we assume a lattice contribution to the specific heat calculated from three Einstein oscillators centered at the optical frequencies of $\varepsilon/k_B \approx 200$, 450, and 800 K.[19] This lattice contribution fits the data very well at high temperature, where both coincide. Due to the fact that an Einstein model is used the low-temperature specific heat (below 50 K) is not fitted. The remaining specific heat, after having subtracted the pure lattice part, is related to the electronic and magnetic contributions to the specific heat. Figure 2 shows the specific heat, once the lattice contribution has been subtracted, in which two anomalies can be clearly observed, the main one at 250 K (charge ordering) and a second one at 150 K (antiferro-

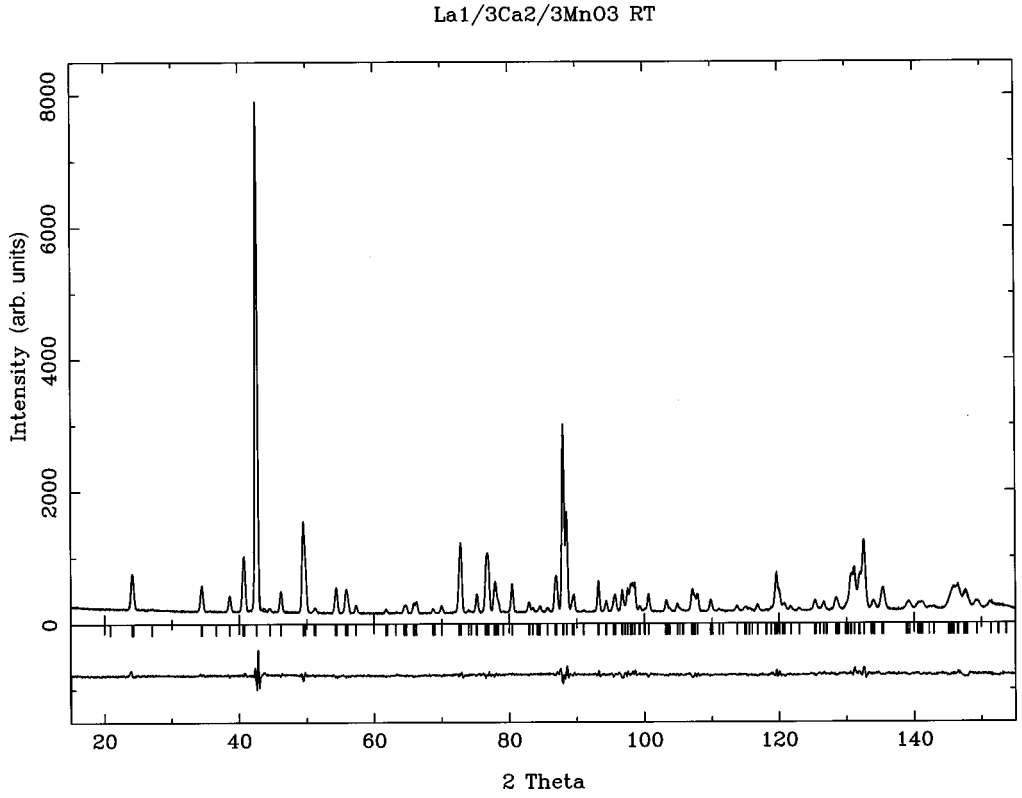

FIG. 3. Observed and calculated neutron powder diffraction patterns for $La_{1/3}Ca_{2/3}MnO_3$ at room temperature.

magnetic ordering). The applied magnetic field (9 T) does not affect the antiferromagnetic order, but displaces the peak associated with the charge ordering only 5 K to higher temperatures and makes it slightly broader.

The analysis of the high resolution neutron-diffraction pattern obtained at room temperature gives a single phase structure with orthorhombic symmetry described by the space group *Pbnm* (standard setting *Pnma*, no. 62) with $b > a > c/\sqrt{2}$, but metrically pseudotetragonal ($b \approx a$). Figure 3 displays the observed and calculated diffraction patterns and the details of the structure are given in Table I, which includes the refined atomic positions, lattice parameters, and temperature factors as well as the different Mn-O distances.

Assuming the Mn site completely occupied, the relative O as well as the La and Ca content were verified by refining the occupation factors of their sites. The stoichiometry found was the nominal one within the standard errors. This is an essential result for the discussion of the physical properties of this compound because they are strongly dependent on the percent Mn^{+4} content. From the calculated Mn-O distances the octahedra distortion can be seen with three different bond lengths, $d(\text{Mn-O}) = 1.925$ and 1.935 Å for the basal plane oxygen ions and 1.919 Å for the apical oxygen, which shows a compressed octahedra.

The behavior of the structure has been followed as the temperature is reduced by sequential refinement of D1B data. For the whole temperature range the average structure has been described in *Pbnm* space group and the atomic positions obtained from the high resolution diffraction data have been used. The dependence of the lattice parameters on temperature from 1.5 K to RT is plotted in the inset of Fig. 4. A smeared phase transition becomes evident from the significant change in the lattice parameters. The orthorhombicity increases ($a \neq b$) and there is an important contraction of the c axis. The change takes place in a wide temperature range and starting around 260 K. This value coincides with the specific heat anomaly, the upturn temperature of the magnetic susceptibility, the onset of the rapid increase of ρ, and the appearance of electron diffraction superlattice spots reported in the literature.[15] As a consequence, all these features should be ascribed to the same underlying mechanism.

We consider that the different effects mentioned originate in a localization process which gives rise to a static state. In this state, the e_g electrons of the Mn^{+3} ions are anchored at specific lattice sites so as from a definite Mn^{+3}-Mn^{+4} pattern. This charge-ordered state gives the additional superlattice spots in the electron-diffraction experiments of Ramirez *et al.* Another consequence of the freezing of carriers is the great increase in the resistivity value, showing that a change in the carrier mobility has occurred. The simultaneous decrease of the magnetization suggests that charge ordering suppresses the ferromagnetic interactions, which are produced by double-exchange mechanism at higher temperatures.

In the neutron diffraction measurements below 170 K several extra peaks appear at low values of the diffraction angle that cannot be indexed on the nuclear cell. Their intensity grows as the temperature is lowered indicating antiferromagnetic ordering of Mn magnetic moments. This transition appears as a bump in the magnetization data around 170 K as well as giving the second broad anomaly in the specific heat measurements, after subtraction of the lattice contribution.

It is interesting to make a brief comparison with the $x = 1/2$ compound. In the case of $La_{1/2}Ca_{1/2}MnO_3$,[20] a ferromagnetic transition takes place at $T = 225$, K and at $T = 155$; K, at the charge-ordering transition, it becomes anti-

TABLE I. Structural data of $La_{1/3}Ca_{2/3}MnO_3$ (*Pbnm*) at RT and 200 K from data collected in D2B with a wavelength of 1.59 Å.

Parameter	$T=300$ K	$T=200$ K
La/Ca $(x,y,1/4)$		
x	0.0055(4)	0.0032(5)
y	0.0213(3)	0.0226(4)
$B(A^2)$	0.80(2)	0.75(3)
Mn (1/2,0,0)		
$B(A^2)$	0.31(2)	0.39(3)
O_p (x,y,z)		
x	0.2795(3)	0.2765(4)
y	0.2782(3)	0.2773(3)
z	0.0313(1)	0.0326(1)
B_{11}	0.0070(2)	0.0144(3)
B_{22}	0.0071(2)	0.0054(2)
B_{33}	0.00331(7)	0.0033(1)
B_{12}	0.0024(2)	0.0021(4)
B_{13}	−0.0001(4)	0.0008(5)
B_{23}	0.0006(4)	−0.0007(4)
O_a $(x,y,1/4)$		
x	−0.0594(3)	−0.0631(3)
y	0.4924(5)	0.4930(5)
B_{11}	0.0085(2)	0.0106(3)
B_{22}	0.0096(3)	0.0071(3)
B_{33}	0.00082(9)	0.0005(1)
B_{12}	0.0007(5)	0.0001(7)
dMn-O_p	1.925(2)	1.933(2)
	1.935(2)	1.939(2)
dMn-O_a	1.9184(3)	1.9069(3)
a (Å)	5.3854 (1)	5.4067 (2)
b (Å)	5.3805 (1)	5.3948 (1)
c (Å)	7.56425 (9)	7.5032 (1)
R_p	3.49	4.79
R_{wp}	4.68	6.33
χ^2 (%)	2.81	3.06
R_{NUCL} (%)	3.67	5.84

ferromagnetic with the magnetic structure reported by Wollan and Koeller.[2] In the present case, the antiferromagnetic ordering takes place at a Néel temperature more than 100 K lower than the charge-ordering transition. This fact seems to indicate that even if the charge-ordering pattern can determine the resulting type of magnetic arrangement, the two phase transitions are decoupled. Nevertheless, as has been reported for the isostructural $Bi_{1-x}Ca_xMnO_3$ in this Mn^{+4} rich regime,[21] the existence of antiferromagnetic fluctuations between the charge-ordering transition and the Néel temperature cannot be excluded. The observed susceptibility inflection can be explained if, at high temperatures, the hopping e_g electron induces ferromagnetic correlations through the double-exchange mechanism and, when these electrons freeze, the ferromagnetic fluctuations are replaced by superexchange driven antiferromagnetic spin fluctuations.

A STRUCTURAL MODEL FOR THE CHARGE-ORDERED PHASE

In order to clarify the kind of change induced in the structure by this electronic phase transition, the refinement of the high-resolution diffraction data measured at 200 K has been made. In our measurements we cannot see any superlattice reflections, and the data seem to fit well with the original *Pbnm* symmetry. However, a clear change is observed in the thermal parameters of oxygen atoms. They are larger and the thermal ellipsoid which, at room temperature, is almost regular in the *xy* plane becomes clearly elongated along the *x* direction at 200 K. This effect could be due to charge ordering leading to displacement of the oxygen atoms in the Mn^{+3}-O_6 octahedra by a static Jahn-Teller distortion.

As the symmetry seems to not change through the transition, when looking for a new space group for this low-temperature phase we begin by considering the isomorphic subgroup of lower index of *Pbnm* which corresponds to a tripling of the cell in one of the three directions. This choice is supported by the superstructure reflections clearly observed by Ramirez *et al.*[15] and by the propagation vector found in the low-temperature results as shown later. The tripling of the structure can take place in either of the two basal directions *a* or *b*. As no superstructure satellites are observed, it is not possible to decide between a $(3a\times b\times c)$ superstructure or an $(a\times 3b\times c)$ one. The development of both models has been undertaken and the results obtained are almost identical for both orientations. However, only one of the options will be presented and the former superstructure type has been chosen, just to be in accordance with the electron diffraction results of Ramirez *et al.* in which a (1/3,0,0) propagation vector was found for the new phase. With this assumption a superstructure model has been built considering a triplication along *a* direction; i.e., $a_{\mathrm{LT}}=3a_{\mathrm{HT}}$, $b_{\mathrm{LT}}=b_{\mathrm{HT}}$, $c_{\mathrm{LT}}=c_{\mathrm{HT}}$. The main feature in that description of the structure is the existence of two different Mn sites, one is the special $4(a)$ site and the other a general $8(g)$ one. From the proportion of Mn^{+4}/Mn^{+3} ions and having in mind quasistatic considerations it seems plausible to place Mn^{+3} ions in the special site with multiplicity 4 and Mn^{+4} ions in the general position with multiplicity 8. Each one of the three other sites in the asymmetric unit of the RT-*Pbnm* symmetry becomes three sets of nonequivalent sites in the new unit cell. As a consequence the new asymmetric unit contains eleven atoms of which four are in general positions, involving 15 atomic-coordinate parameters to fit. For the refinement of that superstructure, it has been assumed as a start fixed parameters for Mn^{+4} sites and refined the rest of the atomic positions considering a random occupancy for La and Ca cation and the position of the three sites related in the following way: Ca/La(1)$=x,y,z$; Ca/La(2)$=x+1/3,y,z$, and Ca/La(3)$=x+2/3,y,z$. The coordinates of the six oxygen positions were refined independently. Then, the temperature isotropic factors have been refined with the following constraints: $B[\mathrm{Ca/La(1)}]=B[\mathrm{Ca/La(2)}]=B[\mathrm{Ca/La(3)}]$; $B(Mn^{+3})=B(Mn^{+4})$; $B(O_p1)=B(O_p2)=B(O_p3)$; and $B(O_a1)=B(O_a2)=B(O_a3)$. Finally the coordinates of Mn^{+4} site have been allowed to vary, using soft constraints in the Mn^{+4}-O distances to obtain a nearly regular octahedron.

The results of the refinement are summarized in Table II, and in Fig. 4 the calculated and experimental patterns are shown. It can be seen that the quality of the fit is almost the same as the one obtained with the average structure. The

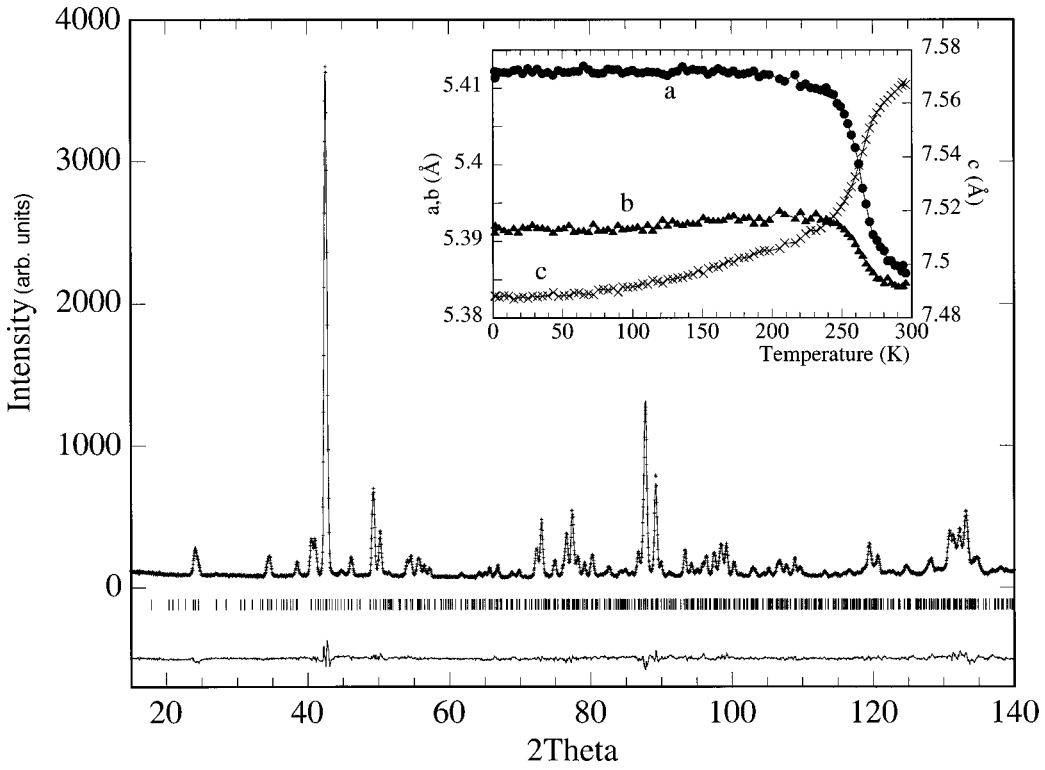

FIG. 4. Rietveld plot of $La_{1/3}Ca_{2/3}MnO_3$ neutron powder diffraction data at 200 K. The refinement results we show correspond to the $Pbnm-(3a_{HT}\times b_{HT}\times c_{HT})$ described in the text. The inset shows the lattice parameters *a*, *b*, and *c* as a function of temperature, obtained from sequential Rietveld refinement of neutron powder diffraction spectra.

number of refined atomic parameters is 19 in the simple cell structure with anisotropic temperature factors for oxygen ions (model I) and 28 in the triple cell model with isotropic temperature factors (model II). In this second case, the *y* coordinates have a high standard deviation. The same thing has been found when supposing a structure model with propagation vector $\mathbf{k}=(0,1/3,0)$, but the indeterminacy in the positions was in that case along *x* direction. This fact could reveal the existence of structural domains with different orientation of the wave vector along the two orthogonal directions of the *x*-*y* plane; i.e., domains of $(3a\times b\times c)$ and $(a\times 3b\times c)$ type. The same effect is observed in the electron diffraction patterns[15] where two orthogonal sets of superlattice spots are found to originate from double domain structure of the charge modulation.

TABLE II. Structural data of $La_{1/3}Ca_{2/3}MnO_3$ at 200 K based on a triple cell model $(3a\times b\times c)$ and keeping the *Pbnm* symmetry.

Atom	*x*	*y*	*z*	*B*
La/Ca(1)	0.0012(7)	0.019(2)	0.25	0.67(3)
La/Ca(2)	0.3387(6)	0.018(2)	0.25	0.67(3)
La/Ca(3)	0.6640(5)	0.029(2)	0.25	0.67(3)
Mn^{+3}	0.5	0	0	0.35(3)
Mn^{+4}	0.1697(5)	−0.0036(7)	−0.0002(4)	0.35(3)
$O_p(1)$	0.0955(3)	0.2709(7)	0.0271(9)	0.76(2)
$O_p(2)$	0.0796(2)	−0.2294(8)	0.0315(9)	0.76(2)
$O_p^{(3)}$	0.2616(2)	0.2127(8)	−0.0405(7)	0.76(2)
$O_a(1)$	−0.0154(3)	0.483(2)	0.25	0.53(3)
$O_a(2)$	0.1931(2)	−0.014(2)	0.25	0.53(3)
$O_a(3)$	0.1448(3)	−0.009(2)	−0.25	0.53(3)
$d Mn^{+3}$-$O_p(1)$	1.9913(46)			
$d Mn^{+3}$-$O_p(2)$	1.9631(40)			
$d Mn^{+3}$-$O_a(1)$	1.8946(8)			
$d Mn^{+4}$-O_a	1.916(9)			
$d Mn^{+4}$-O_p	1.918(40)			
$a=16.2187\,(4)$ Å; $b=5.3948\,(1)$ Å; $c=7.5031\,(2)$ Å				
$R_p=5.00$; $R_{wp}=6.44$; $\chi^2\,(\%)=3.12$; $R_{NUCL}\,(\%)=6.24$				

The most significant change of the structure in the transition is in the Mn-O bond lengths. The Mn-O bond distances resulting from the averaged structure fit (same structure description as above the transition) show a contraction of the apical bond length and two essentially equal in-plane Mn bond distances. Model II was constrained to give six equal Mn^{+4}-O distances, and the Mn^{+3} octahedra has two short bond lengths along the *c* direction of 1.8946 Å, two medium of 1.963 Å, and two long of 1.991 Å in the *ab* plane. From Fig. 5 it is evident that an average of that distribution would give rise to four equivalent in-plane Mn-O distances, in accordance with the results of model I.

MAGNETIC ORDERING

From the position of the extra peaks found at low temperature, a propagation vector for the magnetic structure of (1/3,1/2,0) referred to the RT cell is obtained, which means a propagation vector $\mathbf{k}=(0,1/2,0)$ referred to the low-temperature superstructure. Nevertheless, the magnetic reflections present an asymmetric broadening that prevents from distinguishing between the two possible propagation vectors $\mathbf{k}=(1/2,1/3,0)$ and $\mathbf{k}=(1/3,1/2,0)$ as they do not ex-

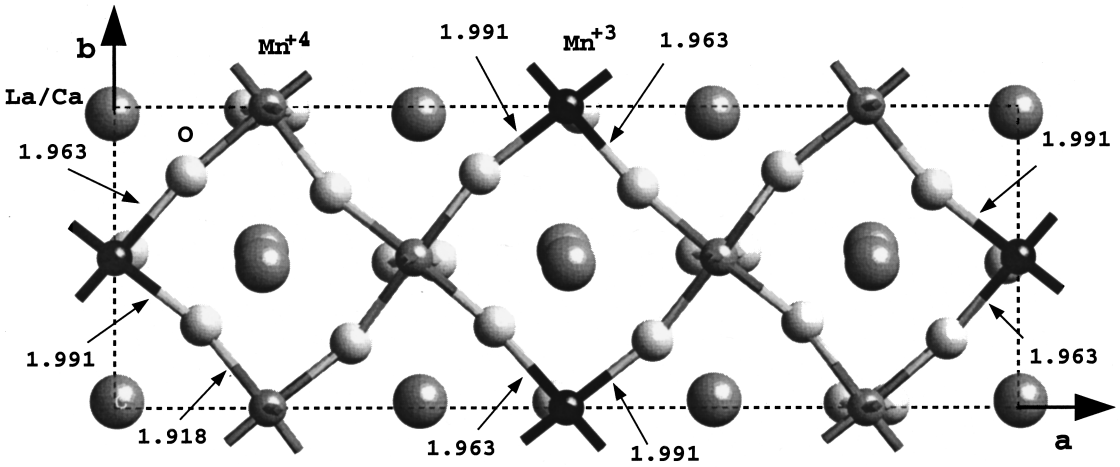

FIG. 5. Scheme of the low-temperature superstructure model for $La_{1/3}Ca_{2/3}MnO_3$ showing the projection in *ab* plane.

actly coincide with the commensurate positions. This broadening may be due to the existence of antiferromagnetic domains separated by stacking faults, corresponding to a change of sign of the magnetic moments in some planes and associated to the presence of planar charge-ordered domains.[20,22]

The arrangement of magnetic moments has been found with the help of group-theory calculations. The vector **k** lies in the first Brillouin zone and it has the full symmetry of the space group ($G_k = Pbnm$). As indicated previously, the magnetic atoms occupy two different sites in the low temperature phase. Mn^{+3} atoms are in a 4(a) position and are numbered in the following way: 1/2,0,0 (1); 1/2,0,1/2 (2); 0,1/2,1/2 (3), and 0,1/2,0 (4). The Mn^{+4} atoms are placed in an $8(g)$ position and labeled: x,y,z (1); $x,y,-z+1/2$ (2); $-x+1/2,y+1/2,-z+1/2$ (3); $-x+1/2,y+1/2,z$ (4); $-x,-y,-z$ (5); $-x,-y,z+1/2$ (6); $x+1/2,-y+1/2,z+1/2$ (7); $x+1/2,-y+1/2,-z$ (8). Using the method developed by Bertaut,[23] the basis vectors associated with $\mathbf{k}=[0,1/2,0]$ have been found in the two-dimensional irreducible representations of space group *Pbnm*. The transformation properties of points $4(a)$ and $8(g)$ generate three sets of basis functions, corresponding to the three directions *x,y,z*. The basis functions separate the Mn^{+4} magnetic sublattice in two sets of related magnetic moments: atoms in 1,2,7,8 and atoms in 3,4,5,6. For each combination of basic functions, the systematic agreement between the observed and calculated diffraction patterns has been checked. The direction of the magnetic moments is found to lie in the *xy* plane. The best agreement is obtained when considering magnetic moments arranged in accordance to the basis function ψ_1 of the Γ_{2k} representation. For the Mn^{+3} sublattice the relationship between the magnetic moments is $S_{1x}-S_{2x}-S_{3x}+S_{4x}$ and $S_{1y}-S_{2y}+S_{3y}-S_{4y}$. For the Mn^{+4} the linear combinations of magnetic moments are $S_{1x}-S_{2x}-S_{7x}+S_{8x}$ and $S_{3x}-S_{4x}-S_{5x}+S_{6x}$; and for the *y* components $S_{1y}-S_{2y}+S_{7y}-S_{8y}$ and $S_{3y}-S_{4y}+S_{5y}-S_{6y}$. The magnetic structure can be described in terms of three independent positions for Mn ions: a Mn^{+3} in (1/2,0,0) and two Mn^{+4} in (1/6,0,0) and in (−1/6,0,0). The magnetic vectors are defined with spherical coordinates and are refined by the modulus of the magnetic moment and the phi angle with the *x* direction, imposing equality of the magnetic moments for the two Mn^{+4} sublattices. The fit is mostly equivalent if considering the magnetic moments of the two Mn^{+4} sublattices related by a rotation of 180° which would correspond to a combination of magnetic moments such as $S_{1x}-S_{2x}-S_{7x}+S_{8x}+S_{3x}-S_{4x}-S_{5x}+S_{6x}$; and for *y* components $S_{1y}-S_{2y}+S_{7y}-S_{8y}-S_{3y}+S_{4y}-S_{5y}+S_{6y}$.

The fit of the experimental pattern at 1.5 K is plotted in Fig. 6. The saturated magnetic moments of Mn^{+3} and Mn^{+4} are respectively 3.4(2) and $2.6(1)\mu_B$ per Mn ion. The usual nuclear and magnetic agreement factors are given in Table III. The sequential fit of D1B diffraction patterns gives the dependence of ordered magnetic moment on temperature; this is plotted in the inset of Fig. 6.

A representation of the plane $z=0$ of the magnetic structure is shown in Fig. 7. The plane $z=1/2$ presents the same ordering pattern antiferromagnetically coupled to the basal plane. That is a noncollinear magnetic structure in which Mn^{+3} magnetic moments are nearly parallel to the magnetic moments of two of their four Mn^{+4} nearest neighbors (the ones along the two long bond lengths of the Mn^{+3}-O_6 octahedron), and almost antiparallel to the other two (the ones along the two medium bond lengths of the Mn^{+3}-O_6 octahe-

TABLE III. Refined magnetic moments of Mn^{+3} and Mn^{+4} ions given in spherical coordinates.

Ion	Magnetic Moment (μ_B)	Phi (degrees)	Theta (degrees)
Mn^{+3}	3.4(2)	−36(6)	90
$Mn^{+4}(1)$	2.6(1)	207(4)	90
$Mn^{+4}(2)$	2.6(1)	51(4)	90

$R_p=4.28$; $R_{wp}=5.69$; χ^2 (%)$=3.99$; R_{NUCL} (%)$=2.34$; R_{MAG} (%)$=13.1$

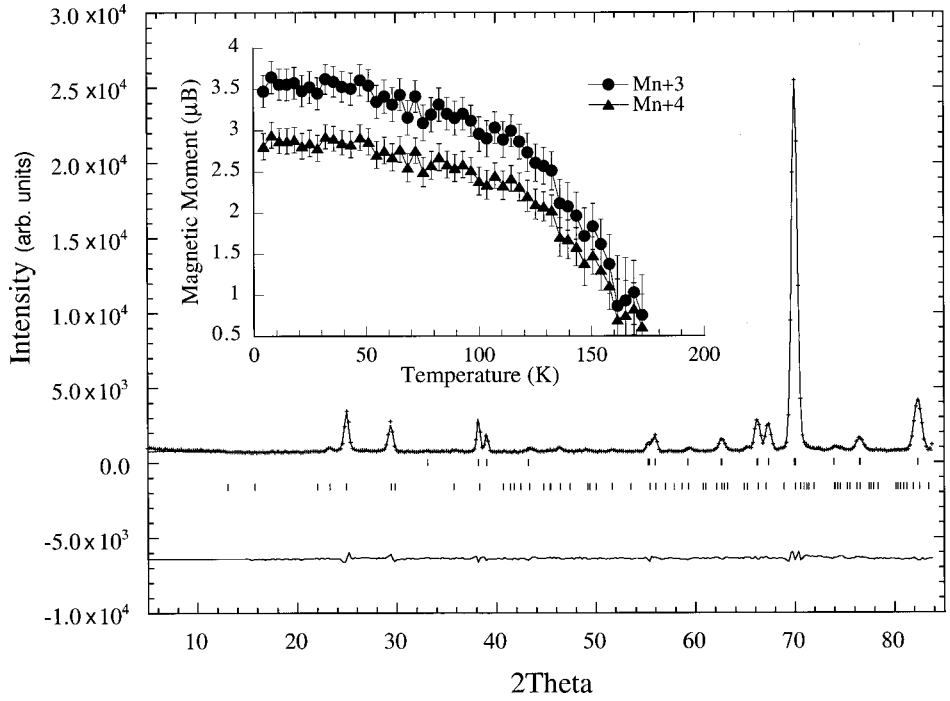

FIG. 6. Observed and calculated neutron powder diffraction patterns for $La_{1/3}Ca_{2/3}MnO_3$ at 1.5 K. The first set of tick marks corresponds to the nuclear phase and the second one to the magnetic phase. The temperature dependence of the ordered magnetic moment for Mn^{+3} and Mn^{+4} ions obtained from the sequential Rietveld refinement of neutron powder diffraction data from D1B is shown in the inset.

dron). On the contrary, the relative orientation of the magnetic moments of two Mn^{+4} nearest neighbors is noncollinear. The existence of ferromagnetic and antiferromagnetic Mn^{+3}-Mn^{+4} exchange interactions cannot be explained in a traditional superexchange model, as there is no way for atoms to couple ferromagnetically in one direction and antiferromagnetically in another. As Goodenough proposed for $La_{1/2}Ca_{1/2}MnO_3$,[6] the charge ordering can be accompanied by an orbital ordering, where the half-filled Mn^{+3} orbitals are associated with long Mn^{+3}-O bonds. This scheme of orbital ordering together with the theory of semicovalence exchange discussed in the Goodenough model allows us to explain the observed magnetic structure.

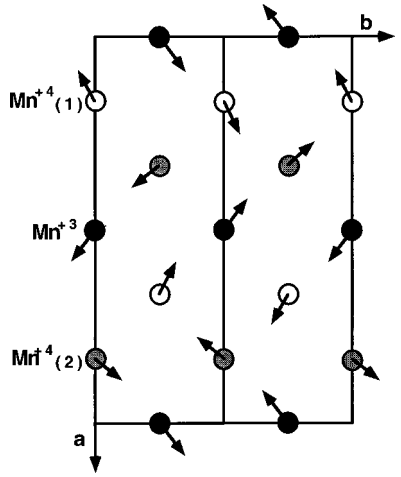

FIG. 7. Proposed antiferromagnetic structure for $La_{1/3}Ca_{2/3}MnO_3$. The drawing shows the $z=0$ plane and only Mn ions have been represented. The magnetic order for the $z=1/2$ plane corresponds to the same kind of structure but coupled antiferromagnetically with the plane shown.

CONCLUSIONS

The electrical, magnetic, thermal, and structural behavior of $La_{1/3}Ca_{2/3}MnO_3$ gives strong evidence for a first order transition to charge-ordered state in this system taking place at temperatures around 270 K. The resulting superstructure would consist of the tripling of the RT cell along *a* or *b* direction. A triple-cell structure keeping the *Pbnm* symmetry allows a plausible model with the distribution of the two types of manganese ions (Mn^{+3} and Mn^{+4}) in two nonequivalent crystallographic sites. Neutron diffraction shows that a further transition to an antiferromagnetic state takes place at $T_N \approx 170$ K. The antiferromagnetic ordering is also clearly observed on the magnetic susceptibility and the excess specific heat. Within the same triple-cell crystallographic model, the resulting magnetic structure has been obtained with the help of group theory calculations giving an antiferromagnetic ordering of the Mn-ions magnetic moments with propagation vector $\mathbf{k}=(0,1/2,0)$ perpendicular to the structural modulation wave vector (1/3,0,0), and belonging to the representation Γ_{2k} of the group *Pbnm* associated with [0,1/2,0] propagation vector.

ACKNOWLEDGMENTS

We would like to thank Dr. J. Rodríguez-Carvajal and Dr. B. Ouladdiaf for helpful discussions. The authors are grateful to Dr. P. J. Brown for critical reading of the manuscript. This work was supported in part by the Spanish CICyT under project MAT96-395.

[1] G. H. Jonker and J. H. Van Saten, Physica (Amsterdam) **16**, 337 (1950); **19**, 120 (1953). Also G. H. Jonker, *ibid.* **22**, 707 (1956).
[2] E. O. Wollan and W. C. Koehler, Phys. Rev. **100**, 545 (1955).
[3] C. Zener, Phys. Rev. **81**, 440 (1951); **82**, 403 (1951).
[4] P. W. Anderson and H. Hasegawa, Phys. Rev. **100**, 675 (1955).
[5] P. G. de Gennes, Phys. Rev. **118**, 141 (1960).
[6] J. B. Goodenough, Phys. Rev. **100**, 564 (1955).
[7] J. Kanamori, J. Phys. Chem. Solids **10**, 87 (1959).
[8] R. von Helmolt, J. Wecker, B. Holzapfet, L. Schultz, and K. Samwer, Phys. Rev. Lett. **71**, 2331 (1993).
[9] Y. Tomioka, A. Asamitsu, Y. Morimoto, H. Kuwahara, and Y. Tokura, Phys. Rev. Lett. **74**, 5108 (1995).
[10] A. Asamitsu, Y. Morimoto, Y. Tomioka, T. Arima, and Y. Tokura, Nature (London) **373**, 407 (1995).
[11] Y. Yamada, O. Hino, S. Nohdo, R. Kanao, T. Inami, and S. Katano, Phys. Rev. Lett. **77**, 904 (1996).
[12] C. H. Chen, S.-W. Cheong, and A. S. Cooper, Phys. Rev. Lett. **71**, 2461 (1993); S.-W. Cheong, H. Y. Hwang, C. H. Chen, B. Batlogg, L. W. Rupp, Jr., and S. A. Carter, Phys. Rev. B **49**, 7088 (1994).
[13] J. M. Tranquada, B. J. Sternlieb, J. D. Axe, Y. Nakamura, and S. Uchida, Nature (London) **337**, 561 (1995).
[14] Y. Morimoto, Y. Tomioka, A. Asamitsu, and Y. Tokura, Phys. Rev. B **51**, 3297 (1995).
[15] A. P. Ramirez, P. Schiffer, S.-W. Cheong, C. H. Chen, W. Bao, T. T. M. Palstra, P. L. Gammel, D. J. Bishop, and B. Zegarski, Phys. Rev. Lett. **76**, 3188 (1996).
[16] C. H. Chen, S.-W. Cheong, and H. Y. Hwang, J. Appl. Phys. **81**, 4326 (1997).
[17] S. Mori, C. H. Chen, and S.-W. Cheong, Nature (London) **392**, 473 (1998).
[18] J. Rodríguez-Carvajal, Physica B **192**, 55 (1993).
[19] A. P. Ramirez, S-W Cheong, and P. Schiffer J. Appl. Phys. **81**, 5337 (1997).
[20] P. G. Radaelli, D. E. Cox, M. Marezio, and S-W. Cheong, Phys. Rev. B **55**, 3015 (1997).
[21] W. Bao, J. D. Axe, C. H. Chen, and S-W. Cheong, Phys. Rev. Lett. **78**, 543 (1997).
[22] A. Guinier, *X-Ray Diffraction in Crystals, Imperfect Crystals, and Amorphous Bodies* (Freeman, San Francisco, 1963), Chap. 7.2.
[23] E. F. Bertaut, Acta Crystallogr., Sect. A: Cryst. Phys., Diffr., Theor. Gen. Crystallogr. **A24**, 217 (1968).